Squeezing the crystalline lattice of the heavy rare-earth metals to change their magnetic order: Experiment and *ab initio* theory

A. Vl. Andrianov and O. A. Savel'eva

Department of Physics, Moscow State University, Moscow 119991, Russia

E. Bauer

Institut für Festkörperphysik, Technische Universität Wien, A-1040 Wien, Austria

J. B. Staunton

Department of Physics, University of Warwick, Coventry CV4 7AL, United Kingdom

Ab initio electronic structure theory finds the type of magnetic order of the heavy rare earths to be correlated directly with the *a* and *c* lattice parameters of their hexagonal-close-packed crystal lattices. We refine our experimental data and obtain magnetic phase diagrams showing magnetic state and transition temperatures versus *a* and *c* for Tb and for the alloy $Ho_{0.4}Gd_{0.6}$. For both systems we mark out the boundaries in *a* and *c* space between incommensurate (helical) antiferromagnetic order and ferromagnetic states and find that these agree very well with the theoretical prediction as well as with each other. These data support the proposition of a universal "crystallomagnetic" phase diagram for the heavy rare earths.

PACS number(s): 75.25.−j, 71.18.+y, 75.30.Kz, 75.50.Ee

The heavy rare-earth hexagonal-close-packed (hcp) metals, either as elements, or alloyed with each other and their transition-metal relative yttrium, are believed to be examples of solids where the geometry of the Fermi surface (FS) determines the type of the magnetic structure via "nesting," as first proposed for Cr by Lomer[1] and for rare-earth metals by Dzyaloshinski.[2] There is a variety of magnetic structures, i.e., helical, sinusoidal, cycloid, fan, etc., which occur under different circumstances in these materials.[3] The characteristic common to all these complex structures is a magnetic wave vector **q**, which is approximately an order of magnitude smaller than the Brillouin zone size, always directed along the hexagonal *c* axis. The standard model of rare-earth electronic structure gives a good qualitative description of the formation and magnitude of the magnetic moments. It has long been understood that these local moments, formed predominantly by the localized *f* electrons, interact with each other by spin polarizing the sea of conduction electrons in which they sit. The Ruderman-Kittel-Kasuya-Yoshida (RKKY) exchange interaction mediated by these conduction electrons is responsible for the magnetic ordering in these metals, and so changes in the shape of the FS are inevitably reflected in the modification of the magnetic exchange and hence affect the type of the resulting magnetic order. Moreover, small changes in the *c* and *a* lattice parameters have a profound effect on the FS and consequent magnetic structure.

Recently, using gadolinium as a prototype for all the heavy rare-earth elements, some of us applied an *ab initio* electronic structure theory to generate a unified magnetic phase diagram, which links unequivocally the magnetic structures that the heavy rare earths form to their lattice parameters.[4] As well as verifying the importance of the *c/a* ratio, we also discovered that the atomic unit-cell volume plays a separate, completely distinct role in determining the magnetic properties. We showed that the trend from ferromagnetism to incommensurate ordering as the atomic number increases across the series is

connected to the concomitant decrease in unit-cell volume caused by the well-known "lanthanide contraction." The comparison with experimental data on the rare-earth elements is very good. Gd is placed in the region of diagram where ferromagnetic ordering is favored, whereas Tb, Dy, Ho, Er, Tm, and Yb are positioned where the magnetic wave vector **q** is incommensurate with the lattice so that helical-like magnetic structures form below a transition temperature. Moreover, estimates of both the values of these wave vectors and the corresponding magnetic transition temperatures agree well with experiment.

The theoretical diagram indicates a region in *c* and *a* space where ferromagnetic and incommensurate magnetic order are nearly degenerate. Tb lies close to this area and a number of Gd alloys such as $Ho_{0.4}Gd_{0.6}$ are also predicted to be nearby. This suggests that, by applying uniaxial strain and/or hydrostatic pressure to these materials, a magnetic transition can be triggered. Prior to this theoretical work the experimentalists amongst us had carried out and published experimental data for a Tb single crystal[5,6] and also the rare-earth solid solution $Ho_{0.4}Gd_{0.6}$ (Refs. 7 and 8) under uniaxial compression tension and hydrostatic compression following on from earlier uniaxial stress experiments on the rare earths, e.g., Ref. 9. In this Brief Report we present a further detailed analysis of this experimental data and compare them carefully with the theory. The good agreement we find is further striking experimental confirmation of this phase diagram and the magnetostructural connection it summarizes.

Our *ab initio* theory includes the effects of thermally induced "local moment" fluctuations on the underlying electronic structure. For low temperatures, calculations of a magnetic material are typically based on an electronic band structure which has a fixed spin polarization. This can be a uniform spin polarization for a ferromagnet or fixed sublattice spin polarizations for an antiferromagnet. With increasing temperature, spin fluctuations must be described which eventually
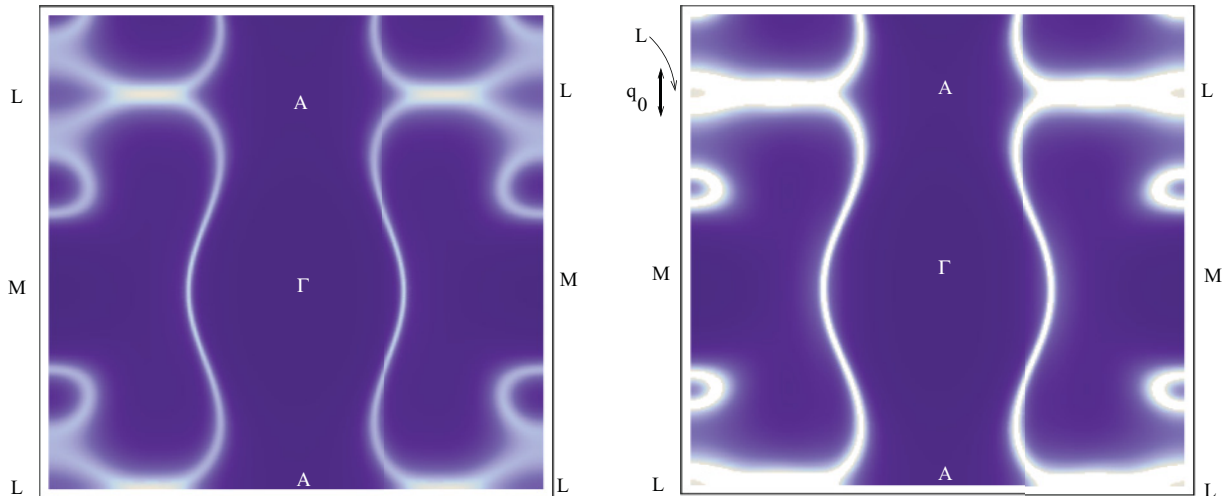
FIG. 1. (Color online) The Bloch spectral function for the ΓLM plane at the Fermi energy for the theoretical paramagnetic rare-earth prototype for a and c values, where the theory indicates (a) ferromagnetic ordering (Gd) and (b) incommensurate magnetic order (Dy). The quantity $\mathbf{q}_0$ indicates the nesting wave vector of the Fermi surface and the shading represents the broadening from the thermally induced local moment disorder.

destroy the long-range magnetic order and the overall spin polarization. For many materials, such as the rare earths, these magnetic excitations can be modeled by associating local spin-polarization axes with all lattice sites and allowing the orientations to vary very slowly on the time scale of the electronic motions. These "local moments" affect the electronic motions and are self-consistently maintained by them. By taking appropriate ensemble averages over their orientational configurations, the system's magnetic properties can be determined. This "disordered local moment" (DLM) density functional theory (DFT)-based theory describes the onset and type of magnetic order *ab initio* in many magnetic systems[10–12] and including an appropriate description of the strongly correlated f electrons[13,14] into this theory enables the studies of Gd and other heavy rare-earth systems to be carried out.[4] An important property of this theory is that a FS can be defined for the paramagnetic state of a metal described in this way. FS nesting can be evident but complicated nonetheless by the local moments which can introduce disorder broadening to the features.

Positron annihilation[15,16] studies of Y and recent angle-resolved photoemission spectroscopy (ARPES) data on Gd, Tb, and Dy (Refs. 17 and 18) have shown further experimental support for the importance of FS nesting for the development of incommensurate antiferromagnetic order. So in this Brief Report we first show from the DLM theory the finite temperature FS of our paramagnetic rare-earth prototype and compare with the experimental data. For a given configuration of local moments this Fermi surface can be defined in the usual way. However, when considering the whole ensemble of moment orientations for a finite temperature description, the "Fermi surface" is a smeared-out average of itself over all moment configurations. A useful tool for defining this surface is the *Bloch spectral function* (BSF),[4,19] $\bar{A}_B(\mathbf{k},E)$, which is periodic in reciprocal wave vector $\mathbf{k}$ space and is given by in terms of an ensemble average of the electronic real-space Green's function. In this case the ensemble average is taken over local moment configurations.[10]

For ordered systems $\bar{A}_B(\mathbf{k},E)$ consists of a set of δ-function peaks,

$$\bar{A}_B(\mathbf{k},E) = \sum_n \delta(E - E_n(\mathbf{k})), \qquad (1)$$

where $E_n(\mathbf{k})$ is the Bloch energy eigenvalue for the wave vector $\mathbf{k}$ and band index n. With disorder (here the local moment spin fluctuation disorder) these peaks broaden, but their positions can be regarded as an effective band structure, with their width in energy interpreted as an inverse lifetime. The Fermi surface of a disordered system is defined as the locus of these peaks at the constant energy $E = E_F$.

Figure 1 shows the Fermi surface for the rare-earth prototype which orders (a) ferromagnetically (lattice parameters of Gd) and (b) with incommensurate magnetic order (lattice parameters of Dy). Figure 1(a) shows no FS nesting whereas a local moment disorder-broadened nesting feature is evident in Fig. 1(b). There is a strong resemblance between our calculations and the ARPES data shown by Dobrich *et al.*[17,18] for paramagnetic states of Gd, Tb, and Dy. [Compare our Figs. 1(a) and 1(b) with Dobrich *et al.*'s Figs. 2(a) and 2(c),[18] respectively.] Both experiment and theory show a prominent nesting structure evident along the L-to-A direction in the Brillouin zone in Dy which is absent in Gd.

In our earlier experimental work we obtained two magnetic phase diagrams for a single crystal of Tb under hydrostatic compression[5] and under uniaxial compression/tension along the hexagonal axis c.[6] We found the values of the a and c crystalline lattice parameters that correspond to the pressures and strains and combined the data into a three-dimensional (3D) plot of the magnetic transition temperature versus a and c. We found the magnetic transition temperature at which the paramagnetic material orders into a helical antiferromagnetic (HAFM) or simple ferromagnetic (FM) phase. We also found where the HAFM transforms into a FM phase at a lower temperature. There is a "triple line" that separates paramagnetic (PM), simple ferromagnetic (FM), and helical
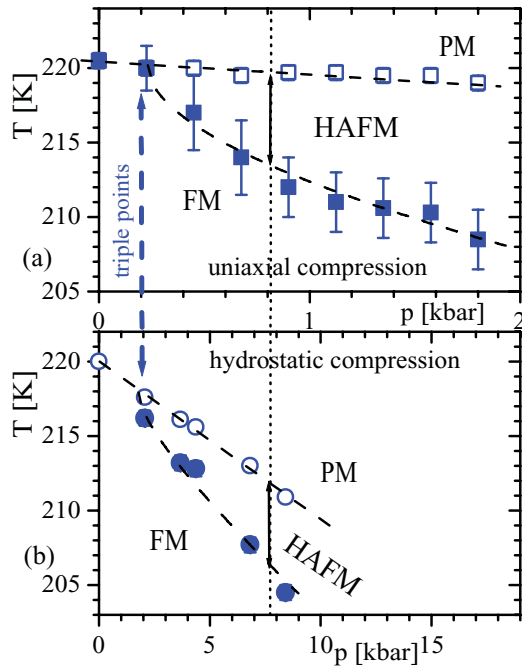
FIG. 2. (Color online) The pressure dependence of the magnetic transition temperatures (a) under uniaxial compression along c axis (squares) and (b) under hydrostatic pressure for $Ho_{0.4}Gd_{0.6}$ (circles). Open dots correspond to the magnetic ordering temperatures T_{ord}, and solid dots to the transition from the helical antiferromagnetic phase to the ferromagnetic one at T_1. Dashed lines are linear fits for T_{ord} and square-root fits for T_1. Abbreviations: PM, paramagnetic; HAFM, helical antiferromagnetic; FM, simple ferromagnetic phases. The pressure scales are adjusted in such a manner that the temperature range where the HAFM phase occurs is the same in both (a) and (b) in the any vertical section with the vertical dotted line as an example. Bold-dashed vertical line marks on both figures indicate the triple points where PM, HAFM, and FM phases meet.

antiferromagnetic (HAFM) phases. Its projection onto the a-c plane provides the boundary between the lattice parameters corresponding to the helical and ferromagnetic magnetic ordering.

Here we show a similar analysis of our data for the single-crystalline rare-earth alloy $Ho_{0.4}Gd_{0.6}$. In contrast with Tb, however, this material orders ferromagnetically at ambient pressure, hence compression was required instead of tension to change the type of the magnetic ordering. A transition from simple ferromagnetic to helical antiferromagnetic order is observed under both uniaxial[7] and hydrostatic[8] pressure. To illustrate this analysis, in Fig. 2 we show the magnetic phase diagrams for uniaxial [Fig. 2(a)] and hydrostatic [Fig. 2(b)] compression. Figure 2(a) is obtained from data in Ref. 7 while Fig. 2(b) is produced from Ref. 8. The pressure dependences of the magnetic ordering temperature T_{ord} are quite linear, its pressure derivatives are -1.05 and -0.88 K/kbar for uniaxial and hydrostatic pressure, respectively, similar to the values for Tb.[5] The pressure dependences of the HAFM-FM "helical phase–ferromagnetic phase" transition temperature T_1 are, in contrast, essentially nonlinear, well described by a square-root dependence (dashed curves).

In Figs. 2(a) and 2(b) the two pressure scales are adjusted in such a manner that the temperature range where the helical

phase occurs is the same in both figures in any vertical section. An example is indicated by the dotted vertical line. This distinct presentation highlights the critical pressure values for the both cases (marked by the dashed vertical line). The respective values for the critical uniaxial and hydrostatic pressures are $p_u^* = 0.2$ kbar and $p_h^* = 1.9$ kbar, respectively, corresponding to magnetic triple points where paramagnetic, helical and ferromagnetic phases match together.

To obtain the lattice parameters a and c at any given pressure, we require their values at ambient pressure as well as elastic moduli values. These moduli for $Ho_{0.4}Gd_{0.6}$ are calculated assuming a linear dependence on the values for pure Ho and Gd:[20] $c_{11} = 0.71$, $c_{12} = 0.25$, $c_{13} = 0.21$, and $c_{33} = 0.75 \times 10^{12}$ dyn/cm^2. The accuracy of these interpolations is acceptable because the values for pure Ho and Gd differ by just $\pm 10\%$. The hcp lattice parameters of $Ho_{0.4}Gd_{0.6}$ at the ambient pressure and at the Curie temperature 220 K were taken from x-ray data for pure Ho and Gd (Ref. 21) linearly extrapolating from the paramagnetic range as $a = 3.608$ Å, $c = 5.716$ Å. Accuracy of these values is believed to be within ± 0.002 Å.

Using these values for ambient pressure and assuming linear stress-strain dependences in the paramagnetic area, we calculate lattice parameters a and c for any given pressure at the magnetic ordering temperature—see Ref. 5 for the details. We compile the 3D "crystalomagnetic" phase diagram by plotting the magnetic transition temperatures versus the corresponding lattice parameters. In this presentation the cases of uniaxial and hydrostatic pressure appear as two cut sets of the single 3D magnetic phase diagram formed by two sheets—one, almost flat, for $T_{ord}(a,c)$ and another nonlinear one for $T_1(a,c)$. These two sheets merge at the "triple line," where paramagnetic, ferromagnetic, and helical phases meet together. The "uniaxial" and "hydrostatic" cut sets coincide when viewed along this "triple line."

We now combine the two sets of data for Tb and $Ho_{0.4}Gd_{0.6}$ to test the theoretical phase diagram. Figure 3 shows the two 3D magnetic phase diagrams on the same plot, viewed in between the two triple lines for each substance. As the directions of these two triple lines are slightly different, the coincidence of the hydrostatic and uniaxial cut sets although not perfect is nevertheless close. We see that these two materials of different chemical content behave remarkably similarly.

By projecting these triple lines onto the a-c plane, we obtain the two boundaries between the lattice parameters corresponding to the helical and ferromagnetic magnetic order—one for Tb and one for $Ho_{0.4}Gd_{0.6}$ (see Fig. 4). The initial values at the ambient pressure and directions of variation of the lattice parameters under respective pressures are added for clarity as well as the triple points for hydrostatic and uniaxial pressures. The positions of these two boundaries coincide within 0.1% accuracy and their slopes are of the same sign and have similar values.

The location of these boundaries is compared directly with the theoretical DLM predictions[4] and is the principal result of this Brief Report. The position of the theoretical boundary is shown in Fig. 4 as green (dash-dot-dot) and yellow (dash-dot) lines, corresponding to the same pseudocolors as in Fig. 3 from the theoretical paper.[4] We see a rather good agreement for Tb and acceptable
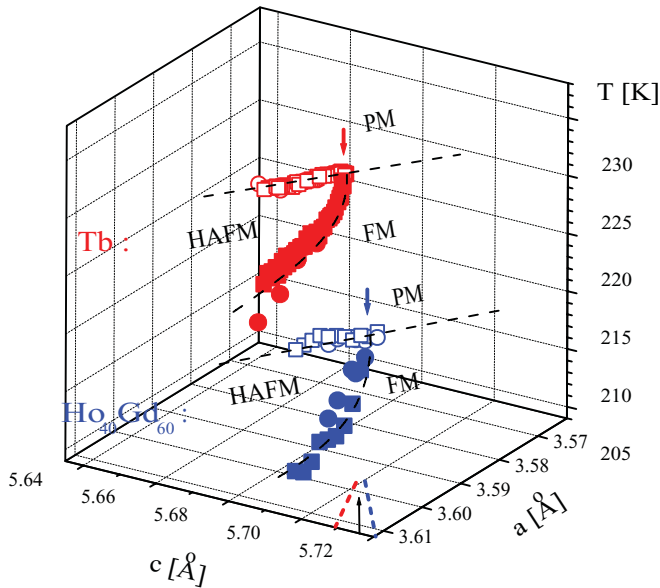
FIG. 3. (Color online) The magnetic phase diagrams of Fig. 2 replotted as magnetic transition temperature vs a and c hcp crystalline lattice parameters for $Ho_{0.4}Gd_{0.6}$ (blue hereafter) and the same for Tb (red hereafter, from Ref. 5), viewed in between their triple lines. Open dots correspond to the magnetic ordering temperatures T_{ord}, and solid dots to the transition from the helical antiferromagnetic phase to the ferromagnetic one at T_1. Squares represent the uniaxial pressure data, and circles for the hydrostatic ones. Dashed lines (guides to the eye) indicate boundaries between magnetic phases. Bold colored arrows indicate the triple points for both substances at both hydrostatic and uniaxial pressures. Bold-dashed lines are projections of triple lines for $Ho_{0.4}Gd_{0.6}$ and Tb onto the a-c plane; arrows mark the projection of the view direction onto the same plane. Note: The angle between these triple lines is exaggerated in this view; see Fig. 4. Abbreviations: PM, paramagnetic; HAFM, helical antiferromagnetic; FM, simple ferromagnetic phases.

FIG. 4. (Color online) Crystallomagnetic phase diagram for $Ho_{0.4}Gd_{0.6}$ (blue hereafter) and Tb (red hereafter), a projection of Fig. 3 onto the the a-c plane. Solid circles show $Ho_{0.4}Gd_{0.6}$ and Tb at ambient pressure and the magnetic ordering temperature. Straight colored arrows indicate the behavior of the lattice parameters under uniaxial and hydrostatic compression calculated employing elastic moduli. Open circles correspond to the magnetic triple points under uniaxial and hydrostatic compression. The bold-dashed lines are projections of the triple lines (the same as in Fig. 3) that separate the ranges of ferromagnetic (FM) and helical antiferromagnetic (HAFM) ordering. Arrows mark the projection of the view direction of Fig. 3. Dash-dot-dot and dash-dot lines present the boundary between these types of the magnetic ordering predicted by *ab initio* theory calculations.

ferromagnetic and incommensurate antiferromagnetic order in a and c space as each other and as the Gd prototype follows in the theoretical calculations. This is strong evidence for a universal crystallomagnetic phase diagram for the heavy rare earths which is set up by the subtle changing topology of their finite temperature conduction electronic structure.

agreement for $Ho_{0.4}Gd_{0.6}$ (note that the result for Tb is more reliable because of the less spread of the initial experimental data and the fewer interpolations made.) We therefore find that two chemically different rare-earth systems can be squeezed to mark out the same boundary between
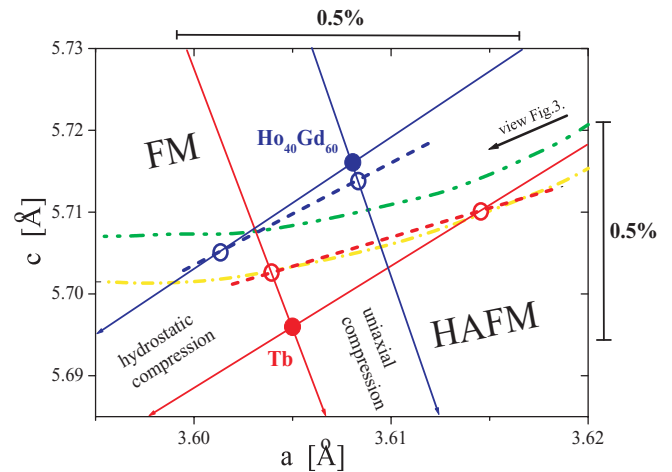
[1] W. M. Lomer, Proc. Phys. Soc. **80**, 489 (1962).

[2] I. E. Dzyaloshinski, Sov. Phys. JETP **20**, 223 (1965).

[3] J. Jensen and A. R. Macintosh, *Rare Earth Magnetism* (Clarendon, Oxford, 1991).

[4] I. D. Hughes, M. Dane, A. Ernst, W. Hergert, M. Luders, J. Poulter, J. B. Staunton, A. Svane, Z. Szotek, and W. M. Temmerman, Nature (London) **446**, 650 (2007).

[5] A. Vl. Andrianov, O. A. Savel'eva, E. Bauer, and Ch. Paul, Phys. Rev. B **72**, 132408 (2005).

[6] A. Vl. Andrianov, D. I. Kosarev, and A. I. Beskrovnyi, Phys. Rev. B **62**, 13844 (2000).

[7] A. Vl. Andrianov and O. D. Chistiakov, Phys. Rev. B **55**, 14107 (1997).

[8] A. Vl. Andrianov and O. D. Chistiakov, Phys. Rev. B **55**, 14107 (1997).

[9] H. Bartholin, J. Beille, D. Bloch, P. Boutron, and J. L. Ferou, J. Appl. Phys. **42**, 1679 (1971).

[10] B. L. Gyorffy *et al.*, J. Phys. F **15**, 1337 (1985); J. B. Staunton and B. L. Gyorffy, Phys. Rev. Lett. **69**, 371 (1992); e.g., V. Crisan, P. Entel, H. Ebert, H. Akai, D. D. Johnson, and J. B. Staunton, Phys. Rev. B **66**, 014416 (2002).

[11] J. B. Staunton, S. Ostanin, S. S. A. Razee, B. L. Gyorffy, L. Szunyogh, B. Ginatempo, and E. Bruno, Phys. Rev. Lett. **93**, 257204 (2004); J. B. Staunton, L. Szunyogh, A. Buruzs, B. L. Gyorffy, S. Ostanin, and L. Udvardi Phys. Rev. B **74**, 144411 (2006).

[12]M. dos Santos Dias, J. B. Staunton, A. Deak, and L. Szunyogh, Phys. Rev. B **83**, 054435 (2011); S. S. A. Razee, J. B. Staunton, L. Szunyogh, and B. L. Gyorffy, Phys. Rev. Lett. **88**, 147201 (2002).

[13]M. Lüders, A. Ernst, M. Däne, Z. Szotek, A. Svane, D. Ködderitzsch, W. Hergert, B. L. Györffy, and W. M. Temmerman, Phys. Rev. B **71**, 205109 (2005).

[14]J. P. Perdew and A. Zunger, Phys. Rev. B **23**, 5048 (1981).

[15]S. B. Dugdale, H. M. Fretwell, M. A. Alam, G. Kontrym-Sznajd, R. N. West, and S. Badrzadeh, Phys. Rev. Lett. **79**, 941 (1997).

[16]S. J. Crowe, S. B. Dugdale, Zs. Major, M. A. Alam, J. A. Duffy, and S. B. Palmer, Europhys. Lett. **65**, 235 (2004).

[17]K. M. Döbrich, A. Bostwick, E. Rotenberg, and G. Kaindl, Phys. Rev. B **81**, 012401 (2010).

[18]K. M. Döbrich, A. Bostwick, J. L. McChesney, K. Rossnagel, E. Rotenberg, and G. Kaindl, Phys. Rev. Lett. **104**, 246401 (2010).

[19]J. S. Faulkner and G. M. Stocks, Phys. Rev. B **21**, 3222 (1980).

[20]M. M. Choy, W. R. Cook, R. F. S. Hearmon *et al.*, *Elastic, Piezoelectric, Pyroelectric, Piezooptic, Electrooptic Constants, and Nonlinear Dielectric Susceptibilities of Crystals*, Landolt–Börnstein Numerical Data and Functional Relationships in Science and Technology, New Series, Group III *Crystal and Solid State Physics*, edited by K.-H. Hellwege and A. M. Hellwege, Vol. 11 (Springer-Verlag, Berlin, 1979), p. 41.

[21]F. J. Darnell, Phys. Rev. **130**, 1825 (1963).